Design and test of a multi-edge toothed cutting device for membrane-impurity mixed material

Rongqing Liang[1,3,4†], Bingcheng Zhang[1,3†], Xuegeng Chen[1,3], Hewei Meng[1,3], Xinzhong Wang[2], Congju Shen[1,3], Yaping Li[1,3*], Za Kan[1,3]

(1. *College of Mechanical and Electrical Engineering, Shihezi University, Shihezi 832000, Xinjiang, China*;
2. *School of Agriculture Engineering Jiangsu University, Zhenjiang 212013, Jiangsu, China*;
3. *Engineering Research Center for Production Mechanization of Oasis Special Economic Crop, Ministry of Education, Shihezi 832000, Xinjiang, China*;
4. *College of Energy and Machinery, Dezhou University, Dezhou 253023, Shandong, China*)

Abstract: As the existing residual film crushing device in Xinjiang cannot directly crush membrane-impurity mixed material, by analyzing the compressive and cutting force characteristics of residual film material layer and cotton stalk, the cutting conditions of mixed materials were obtained, and the method of cutting was determined. A multi-edge toothed cutters was created, and a cutting device was built. It was preliminarily determined that the number of teeth in the cutters was 8, the clearance between the teeth and between the tooth and fixed blade was 3 mm, the speed of the high-speed cutter was 800 r/min, and the speed difference between the high- and low-speed cutters was –300 r/min. Test results show that the ratio of residual film to total residual film sampling mass was (2.22±0.30)%, (19.19±2.02)%, (58.94±3.19)% and (20.65±2.05)%, respectively, when the maximum outer profile size in the range of [0,20) mm, [20,100) mm, [100,500) mm and [500,~) mm. The mass of cotton stalks with lengths of [0,50) mm, [50,100) mm and [100,~) mm accounted for (32.57±1.5)%, (27.77±1.3)% and (39.66±1.75)%, respectively, and the cutting power consumption was (85.41±15.63) kJ. The test results can provide a basis for the subsequent membrane-impurity mixed material cutting technology, as well as some guidance for the separation of it.

Keywords: Multi-edge toothed cutter, membrane-impurity mixed material, cutting device, cutting conditions
DOI: 10.25165/j.ijabe.20231602.7240

Citation: Liang R Q, Zhang B C, Chen X G, Meng H W, Wang X Z, Shen C J, et al. Design and test of a multi-edge toothed cutting device for membrane-impurity mixed material. Int J Agric & Biol Eng, 2023; 16(2): 73–84.

1 Introduction

With the combination and wide applications of plastic film mulching technology, dwarfing and density planting technology, and drip irrigation technology, Xinjiang has become the leading cotton growing region[1,2]. Moreover, the plastic films mulching technology has increased the cotton yield year by year, enabling Xinjiang to harvest more cotton than ever before. However, soil contamination and environmental pollution caused by residual plastic film have become increasingly serious[3,4]. There have been more contradictions among the use of plastic film in farmland, the protection of agricultural crops and the ecological environment, and the green and sustainable development of modern agriculture[5]. At present, most of the mulch films covering the soil of farmland are petroleum-based polymers. Reasonable and applicable ways for residual film recovery，initial cleaning and resource utilization are strong guarantees for reducing pollution and improving resource utilization[6,7]. The popularization and applications of residual film mechanical recovery technology has alleviated the problem of residual film pollution in Xinjiang cotton fields to a certain extent, and promoted the effective utilization of residual films. However, affected by many factors such as the thickness, strength and recycling method of mulch films[8], the recycled residual films contain a large number of cotton stalks and soil-based impurities[9], forming a complex structure and mechanical characteristics. The unique characteristics of the membrane-impurity mixed material have therefore increased the difficulty of initial cleaning and resource utilization.

Initial cleaning is the primary link in the effective utilization of residual membranes. In order to efficiently use membrane-impurity mixed material, extensive research has been conducted on the key technologies of initial cleaning. Domestic scholars, however, have only studied separation technologies and equipment mainly with method of vibration screening, suspension water washing and wind separation[10-12], while paying few attention to the cutting technology. Pan et al.[13] developed a kind of curved arc V-type hob type membrane-impurity mixed material cutting device, explained its working process and characteristics, and obtained the cutting performance of the device. Liang et al.[14,15] obtained the main factors affecting the power consumption and the distribution characteristics of cotton stalk length in mixed materials after cutting, and analyzed

Received date: 2021-12-05 **Accepted date:** 2023-02-20
Biographies: Rongqing Liang, PhD, research interest: agricultural engineering technology, Email: liangrongqing2008@163.com; **Bingcheng Zhang**, PhD Candidate, research interest: agricultural engineering technology, Email: 1414787465@qq.com; **Xuegeng Chen**, Professor, research interest: agricultural engineering technology, Email: chenxg130@sina.com; **Hewei Meng**, PhD Candidate, research interest: agricultural engineering technology, Email: mengbai4251982@sina.com; **Xinzhong Wang**, Professor, research interest: agricultural engineering technology, Email: xzwang@ujs.edu.cn; **Congju Shen**, Associate Researcher, research interest: agricultural engineering technology, Email: shencongju@163.com; **Za Kan**, Professor, research interest: agricultural engineering technology, Email: kz-shz@163.com.
†These authors contributed equally to this work.
***Corresponding author: Yaping Li**, Professor, research interest: agricultural engineering technology. College of Mechanical Electrical Engineering, Shihezi University, Shihezi 832000, China. Tel: +86-15299911288, Email: liyaping425@163.com.

the influence law of key parameters of the device on the power consumption and distribution characteristics of cotton stalk length. As the primary link of initial cleaning and the necessary link of resource utilization[16], cutting technology is one of the important factors to ensure the effects of separating membrane-impurity mixed material and the quality of the regenerated products of residual membranes. At present, the plastic cutting equipment was used in Xinjiang to cut residual film with fewer impurities, but it is not completely suitable for direct cutting of membrane-impurity mixed material. Therefore, it is urgent to carry out research and development of cutting technologies and equipment suitable for membrane-impurity mixed material.

In view of this, combined with the characteristics of membrane-impurity mixed material in Xinjiang, based on the analysis of the cutting conditions of cotton stalks and residual film material layers, a multi-edge toothed cutting device for separating membrane-impurity mixed material was designed. The value range of key parameters such as the number of teeth in the cutters, the clearance between the teeth and between the tooth and fixed blade, the speed of high-speed toothed rollers, the speed difference between high-speed and low-speed toothed rollers were determined. On this basis, a physical test was performed using evaluation indexes like the distribution characteristics of the maximum outer profile size of the residual film, the distribution characteristics of the cotton stalk length and the cutting power consumption, with the purpose of investigating the working performance of the cutting device, and thus providing some theoretical reference and technical support for the development of film cutting equipment in Xinjiang.

2 Analysis of cutting conditions of membrane-impurity mixed material

The cutting direction of the stem by the cutters can be divided into three types: transverse cutting, oblique cutting and tilted cutting. Compared with oblique cutting and tilted cutting, transverse cutting has the largest cutting resistance[17]. Without considering the power consumption, if the external force on the stem is greater than the force of transverse cutting, other cutting methods can also be achieved. When the membrane-impurity mixed material is cut, the granular material dominated by soil can be not considered, because of its particle size is too small to influence the cutting performance. The axis of the cotton stalk is uncertain relative to the cutting direction of the cutting tool, resulting in certain randomness of the transverse cutting, oblique cutting and tilted cutting of the cotton stalk. In view of this, the cutting conditions of the cotton stalk and the residual film are analyzed under transverse cutting conditions.

2.1 Analysis of Cotton stalk Cut Conditions

Cotton stalks are a non-rigid material that may deform under the action of external forces. When a cotton stalk is chopped by a transverse cutting, the moving direction of the cutting tool is perpendicular to the axis of the cotton stalk, and it will be completely cut off after extrusion deformation and cutting deformation. Therefore, the extrusion deformation and cutting deformation stress characteristics of the cotton stalk in the cutting process were analyzed.

As shown in Figure 1, when the cutting tool contacted the cotton stalk, the cotton stalk was subjected to external forces, extruded and deformed to some degree. In order to obtain the contact stress and extrusion deformation of the cotton stalk in the extrusion deformation stage, stalk contact mechanics in reference [18] was employed. It was assumed that under the force of the cutting tool, the stress of the cotton stalk after deformation mainly acted on the elliptical contact area with half axes a and b. According to Hertzian contact theory[19], the equivalent contact radius of the elliptical contact area is:

$$c = \sqrt{ab} = \sqrt[3]{\frac{3FR_e}{4E^*}} \cdot F(e) \tag{1}$$

where, a and b are the long-axis diameter and short-axis diameter of the elliptical contact area, m; c is the contact radius of the elliptical contact area, m; F is the external force, N; R_e is the relative radius of the curvature, m. E^* is the Young's modulus; e is the ratio of relative curvature radius at both ends of the contact; $F(e)$ is the correction coefficient.

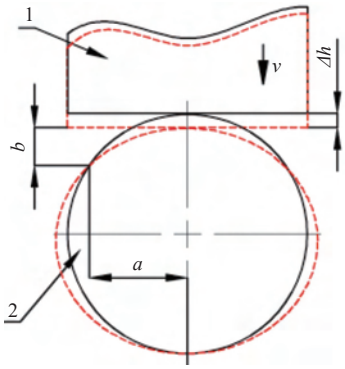

1. Cutting tools 2. Cotton stalk

Figure 1 Diagram of extrusion deformation stage of cotton stalk

According to the contact mechanics theory, the ratio of E^* to e in Equation (1) can be expressed as:

$$\begin{cases} E^* = \dfrac{E_1 \cdot E_2}{E_1(1-\upsilon_2^2) + E_2(1-\upsilon_1^2)} \\ e = \sqrt{\dfrac{1-b^2}{a^2}};\ b < a \end{cases} \tag{2}$$

where, E_1 and E_2 are the Young's moduli of the cutting tool and the cotton stalk, respectively; υ^1 and υ^2 are Poisson's ratios of the cutting tool and the cotton stalk, respectively.

In addition, as per Hertzian contact theory, under the action of external force F, the maximum compression of the cotton stalk in the elliptical contact area can be expressed as:

$$\begin{cases} F_{\max} = \dfrac{3F}{2\pi ab} = \sqrt[3]{\dfrac{6FE^{*2}}{\pi^3 R_e^2 F(e)^2}} \\ \delta = \sqrt[3]{\dfrac{9F^2}{16R_e E^{*2}}} \cdot F'(e) \end{cases} \tag{3}$$

where, $F_{\max}$ is the maximum contact pressure; N; δ is the maximum compression of the elliptical contact area, m; $F'(e)$ is the correction coefficient.

As shown in Figure 2, it was assumed that the double-edged cutter was used to cut the cotton stalk with diameter of R, r is the cut quantity. In accordance with the material layer cutting theory in reference [20], the stress characteristics of the cotton stalk were analyzed. The coordinate system $x'o'y'$ was constructed by taking the blade surface as x'-axis. The reaction force of cotton stalk on the blade surface is:

$$F_d = F_x \cos\frac{\theta}{2} + F_y \sin\frac{\theta}{2} \tag{4}$$

where, F_d is the force reacting vertically to the blade surface, N; F_x is the force acting on the blade surface perpendicular to the moving

direction of the cutting tool, N; F_y is the force acting on the blade parallel to the moving direction of the cutting tool, N; θ is the angle between the blade faces on both sides of the cutting tool, (°).

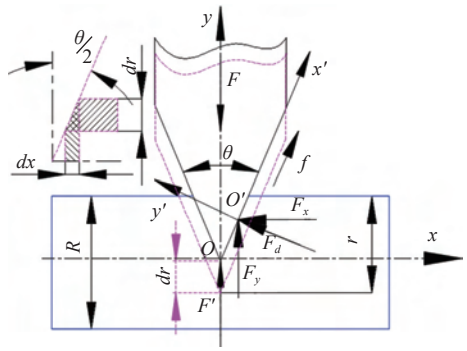

Figure 2 Diagram of cotton stalk cutting deformation stage

According to the principle of friction between materials, the friction f between the cotton stalk and the blade surface under external forces can be expressed as:

$$f = \mu_s F_d = \mu_s \left(F_x \cos\frac{\theta}{2} + F_y \sin\frac{\theta}{2} \right) \tag{5}$$

where, f and μ are the friction force and the friction coefficient between the cotton stalk and the blade respectively.

The *xoy* coordinate system was established with the vertex o of the cutting tool at the origin. The force balance equation for the cutting tool moving direction along the *y*-axis is:

$$F = 2F_y + F' + 2f\cos\frac{\theta}{2} \tag{6}$$

where, F is the force of the cutting tool on the cotton stalk, N; F' is the reaction force of the cutter to extrude the cotton stalk at the apex o, N.

In addition, it was assumed that the thickness of the double-edged cutting tool was e and the blade length was l. Conforming to the compression deformation theory in classical mechanics, F' is solved as follows:

$$F' = Eel\frac{\zeta}{R} \tag{7}$$

where, E denotes the elastic modulus of cotton stalk, MPa; e stands for cutting tool's blade thickness (e=50-150 μm[21]), m; l is the unit length of the cutting tool blade, m; ζ is the cutting deformation height in the range of 0-R, m.

As the cutting tool moved down, the contact area between the blade surface and the cotton stalk increased gradually. As shown in Figure 2, the cutting tool moved dr in the *y-axis* direction and the blade surface moved dx in the *x-axis* direction, assuming that the cotton stalk unit was isotropic in the *x-axis* and *y-axis*. It can be seen from Equation (7) that in the *x-axis* and *y-axis* directions, the force of cotton stalk reacting on the blade surface unit is:

$$\begin{cases} \mathrm{d}F_x = \dfrac{Eldr}{R}\mathrm{d}r \\ \mathrm{d}F_y = \dfrac{Eldr}{R}\mathrm{d}r\cdot\tan\dfrac{\theta}{2} \end{cases} \tag{8}$$

The integral equation of the force acting on the cotton stalk in the *x*-axis and *y*-axis directions at any point ζ in the range of 0-R can be expressed as:

$$\begin{cases} F_x = \int_0^{\zeta} \dfrac{El}{R}\mathrm{d}r^2 \\ F_y = \int_0^{\zeta} \dfrac{El}{R}\tan\dfrac{\theta}{2}\mathrm{d}r^2 \end{cases} \Rightarrow \begin{cases} F_x = \dfrac{El\zeta^2}{2R} \\ F_y = \dfrac{El\zeta^2}{2R}\tan\dfrac{\theta}{2} \end{cases} \tag{9}$$

According to Equation (6), if the cotton stalk is completely cut off, the force in the *y-axis* direction would be:

$$F \geqslant 2F_y + F' + 2f\cos\frac{\theta}{2} \tag{10}$$

Bring Equations (5), (7) and (9) into (10) to:

$$F \geqslant \frac{El\zeta^2}{R}\tan\frac{\theta}{2} + \frac{Eel\zeta}{R} + \mu\frac{El\zeta^2}{R} \tag{11}$$

It can be seen from Equation (11) that the material characteristics of the cotton stalk, the friction characteristics between the cotton stalk and the cutting tool, as well as the shape and structure of the cutting tool all affect the required external force when cutting. Due to the small extrusion deformation of the cotton stalk, the cutting resistance is mainly concentrated in the cutting process. Therefore, the cutting efficiency can be improved by increasing the cutting tool speed, external force and reducing the tool angle.

2.2 Analysis of residual film cutting conditions

The residual film is a petroleum-based polyethylene or polyvinyl chloride product[22]. The thickness of a single residual film is only 0.01 mm (the nominal thickness of the current mulch film in Xinjiang), but the accumulated residual film material layer is relatively fluffy and the volume is large. It should be fully extruded before entering the cutting stage. As shown in Figure 3, it was assumed that the residual film material layer units changed only in the height direction during the extrusion deformation process. Under the action of the external force F_n, its height reduced h from the original h_0 after being compressed, while the width and length remained a and b. That is, its surface area A remained unchanged. According to Hooke's law[23], the F_n is:

$$F_n = E_c A\frac{\xi}{h_0} \tag{12}$$

where, F_n is the external force, N; E_c is the elastic modulus of residual film, MPa; A is residual film material layer unit stress cross-sectional area, m^2; ξ is the arbitrary deformation of 0-h in the compression process of residual film material layer, m; h_0 is the original height of residual film material layer unit, m.

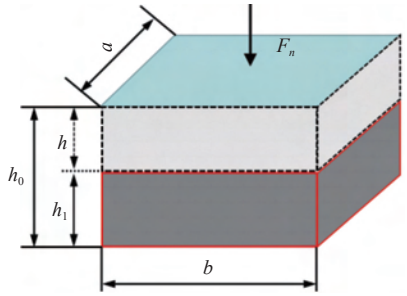

Figure 3 Extrusion deformation of residual film layer element

When the residual film material layer unit was not compressed, namely ξ=0, the external force F_n=0. When compressed to h, which is ξ=h, it can be obtained:

$$F_n^h = \frac{E_c Ah}{h_0} \tag{13}$$

After extrusion deformation (i. e., h_1=h_0−h), the residual film material layer unit began to cutting deformation, which was similar to the cotton stalk. As shown in Figure 4, it was assumed that the residual film layer is isotropic and it was cut off by a double-edged cutter. If the residual film material layer was cut off, the force of the residual film material layer on the *y*-axis would be:

$$F_c \geqslant \frac{E_c l\iota}{h_1}\left(\iota \tan\frac{\theta}{2}+e+\iota\mu_c\right) \quad (14)$$

where, F_c is the shear force of the cutter on the residual film layer, N; l is the shear deformation height in the range of 0-h_1, m; μ_c is the coefficient of friction between the residual film and the tool; h_1 is the height of the residual film after complete extrusion deformation, m.

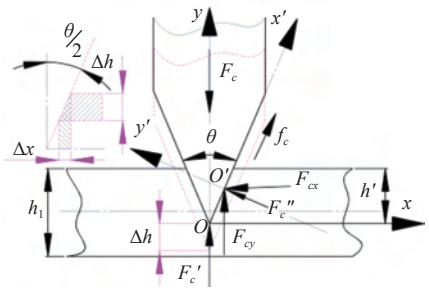

Figure 4 Shear process of residual film layer element

It can be seen from Equation (14) that when the cutter is used to cut the residual film material layer, the thickness of the material layer, the friction characteristics between the material layer and the cutter, as well as the shape of the cutter will affect the cutting effect. In addition, the residual film with the good flexibility is extremely unfavorable for cutting, because the residual film will produce large deformation while moving with the cutter. Therefore, it is necessary to avoid using non-support cutting methods dominated by impact to cut the residual film. Instead, the support cutting method was selected, and the sharper cutter was selected as far as possible, so as to shorten the compression deformation time and improve the transfer efficiency of external force, as well as ensure that the residual film in a smaller external force to achieve shredding.

3 Analysis of structure characteristics and working characteristics of cutting device

3.1 Structural characteristics of cutting device

According to different cutting principles, the cutter is divided into supported and unsupported. Unsupported cutting mainly realizes material cutting or crushing by instantaneous impact force generated by high-speed rotary cutters. Literature suggests that cotton stalk cellulose and lignin accounted for about 46% and 26%[24], respectively. Compared with other crop straws, cotton stalks have a higher lignification degree, better hardness and stiffness. Therefore, the impact-based unsupported cutting is often used, and cotton stalks are crushed by hammer, flail knife or hob[25-29].

Luo et al. and Sakai et al. studied the crushing characteristics of municipal waste consisting mainly of flexible materials, and believed that the impact force was easily absorbed by flexible materials and could not be effectively transferred, so the hammer-type crushing device should be avoided[30,31]. In addition, Vincent et al. and Maisel et al. studied the crushing characteristics of thermoplastic material products, and noted that the roll crusher with supported cutting mainly could effectively crush the thermoplastic material products with good crushing quality and uniform material sizes[32,33].

In view of this, based on the analysis of cotton stalk cutting process and residual film material layer cutting conditions, taking into account the characteristics of the two materials, the rotary cutting mechanism was selected to cut the film mixture. A multi-edge toothed cutting device for membrane-impurity mixed material was designed, as shown in Figure 5. The device was mainly composed of a power and transmission system, cutting parts, a feed inlet, a discharge outlet and a frame.

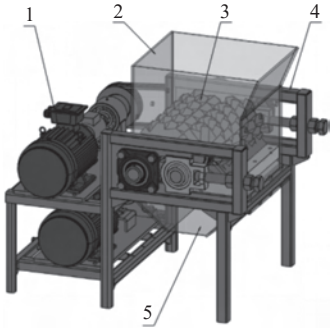

1. Power and transmission system 2. Feed inlet 3. Chop parts 4. Frame 5. Discharge port

Figure 5 Structure diagram of the multi-edge tooth cutter type cutting device for membrane-impurity mixed material

3.2 Analysis of working characteristics of cutting device

In Figure 6, the working process of the cutting device is as follows: the power and transmission system provided power for the device, and drove the high- and low-speed toothed rollers to rotate reversely at the speeds of n_1 and n_2. At this time, the membrane-impurity mixed material fed by the feed port fell into the extrusion zone *I*. The high- and low-speed toothed rollers rotated to drive the material to the staggered cutting extrusion zone *II*, and part of the smaller granular material was directly discharged through the clearance between the multi-edge toothed cutters through the discharge port.

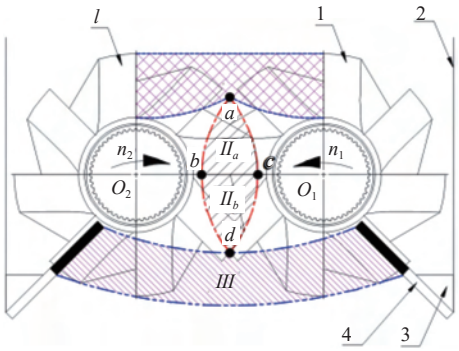

1. Multi-edge cutter 2. Cut cavity wall 3. Setting knife 4. Setting knife seat I: Extrusion region II: Interlaced cutting extrusion region III: secondary cutting region

Figure 6 Working characteristics of the cutting device for membrane-impurity mixed material

With the rotation of the two toothed rolls, the multi-edge toothed cutter on the rolls continuously squeezed the material into the staggered cutting extrusion zone *II*. After the rake face of the multi-edge toothed cutter passed point *a*, it completely entered the staggered cutting extrusion area. In this area, the multi-edge toothed cutter on the high- and low-speed toothed roller interacted to cut and squeeze the film mixture. After passing point *d*, the multi-edge toothed cutter completely entered the secondary cutting area *III*. In this area, the multi-edge toothed cutter drove the reverse movement of the residual film that was not cut off or had a large outer profile size to realize the residual film stretching and tearing. In addition, the residual film with superior ductility or winding on the multi-edge toothed cutter might be brought to the fixed cutter, and the multi-edge toothed cutter and the fixed cutter interacted to secondary cutting and stripping.

4 Design of key components and determination of parameters of cutting device

The cutting part (Figure 7) is the core component of the multi-edge toothed cutting device for membrane-impurity mixed material. It is mainly composed of pulley 1, multi-edge toothed cutter 2, clearance adjusting mechanism 3, low-speed roller 4, slide bearing with seat 5, bearing with square seat 6, high-speed roller 7, fixed cutter seat 8 and fixed cutter 9.

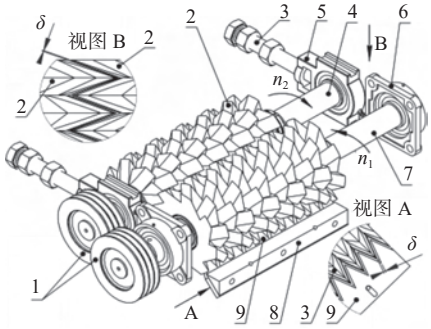

1. Pulley 2. Multi-edge toothed cutter 3. Clearance adjusting mechanism 4. Low-speed roller 5. Slide bearing with seat 6. Bearing with square seat 7. High-speed roller 8. Fixed cutter seat 9. Fixed cutter

Figure 7 Structure diagram of test device cutting parts

Multi-edge toothed cutter 2, high-speed shaft 7 and low-speed shaft 4 constitute high- and low-speed toothed rollers respectively. 10 toothed cutters were evenly arranged on the two shaft (two half multi-edge toothed cutters on both ends of the rollers were regarded as a whole), and the multi-edged toothed cutters on the high-speed roller and the low-speed roller were staggered. Adjusting the center distance between the two rollers can realize the clearance adjustment between the multi-edge toothed cutters. In addition, the clearance between the fixed cutter and the multi-edge toothed cutter can be realized by adjusting the relative position between the fixed cutter and the fixed cutter seat by bolts.

4.1 High- and low-speed cutting tooth roller structure characteristics and working parameters

A high-speed toothed roller shares a similar structure with a low-speed one. They are both mainly composed of a multi-edge toothed cutter, a roller, a seat bearing (high-speed toothed roller is matched with square seat bearing, low-speed cutting tooth roller is slide bearing with seat), a spacer, a round nut and a pulley and other parts (Figure 8).

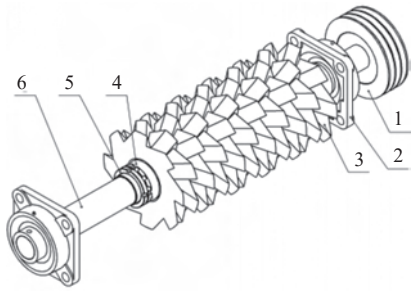

1. Pulley 2. Bearing with square seat 3. Multi-edge toothed cutter 4. Spacer 5. Round nut 6. High-speed roller

Figure 8 Structure diagram of the high-speed cutting gear roller

The rotational speed is an important factor affecting the material cutting effect[34]. When the rotational speed is high, the instantaneous impact force will be large, which is conducive to cutting materials, but the power consumption is also high. When the rotational speed is low, the instantaneous impact force will be small. Although it is conducive to energy saving and consumption reduction, the material cutting effect also decreases, and even the material feeding amount will be too large or the feeding speed will be too fast to cause blockage. According to literature [17], the line speed could be appropriately reduced when use support cutting. In reference [35], when the rotary cutter was used to cut the grain stalk, the value range of line speed of cutter was 6-16 m/s. In this case, it was preliminarily determined that the line speed v_n of the high-speed toothed roller was 11 m/s. Reference [36] shows that the maximum speed of the new plastic crushing device was 1000 r/min. Therefore, it was preliminarily determined that the speed n_1 of the high-speed roller was 800 r/min, and the outer diameter of the high-speed roller was:

$$D = \frac{60v_n}{\pi \cdot n_1} \tag{15}$$

where, n_1 is the speed of the high-speed toothed roller, r/min; v_n is the line speed, m/s; D is the outer diameter of high-speed toothed roller, m.

In accordance with Equation (15), the outer diameter of the high-speed toothed roller is 263 mm, and the diameter of the rounding is 260 mm, which is the diameter of the top edge of the multi-edge toothed cutter.

The principle of rotational speed difference was widely used in many agricultural production processes[37,38]. References [39] and [40] have shown that the action characteristics of rotational speed difference when interact with materials were better than those at the same speed. The existence of the speed difference made the high- and low-speed toothed rollers cutting like the fixed and moving cutters, which was the same as the interaction characteristics of the rotating cutter and the fixed, thereby being beneficial to the cutting of the mixed material. In the agricultural machinery design manual, it is proposed that the speed difference between the two rollers in the sawtoothed roller of corn kernel crushing system was 20%[40]. Liu et al. used a speed difference styled straw returning machine to crush corn straws, and set the speed of the sliding support knife as 1/2 of the speed of the knife for picking up and crushing[41]. Overall, the rotational speed of the low-speed toothed roller was initially determined to be 500 r/min, which suggested that the speed difference Δn between the high- and low-speed toothed rollers was –300 r/min.

In addition, as shown in Figure 9, at any point m in the staggered cutting extrusion region I, the corresponding diameters of the high- and low-speed toothed rollers are D' and D'', respectively. It can be seen from Equation (15) that the rotational speeds of high-

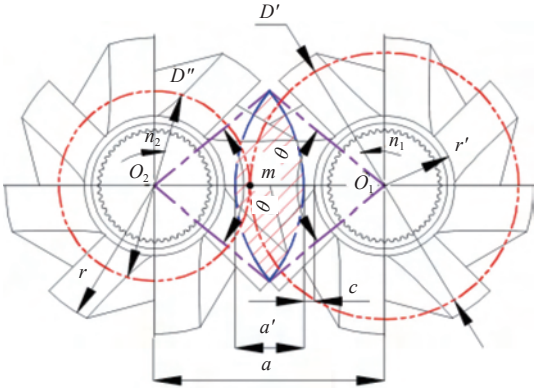

Figure 9 Center-to-center distance between the high- and low-speed cutting tooth rollers

and low-speed toothed rollers at point m are n' and n'', respectively, indicating that there is a rotational speed difference at point m[39], which is conducive to the cutting of membrane-impurity mixed material.

4.2 Structure characteristics of Multi-edge toothed cutter

The multi-edge toothed cutter is an important component of the high- and low-speed toothed rollers (Figure 10). It mainly includes a rack face 1, a rear face 2, a flank face 3, a front blade 4, a back blade 5, a top blade 6, a knife hub 7 and an integral key 8. Double supported cutting for the membrane-impurity mixed material is performed between the rack face 1, back blade 5 and top blade 6 as well as the fixed cutters, and the adjacent flank face 3 interact to extrude the membrane-impurity mixed material. The knife hub 7 ensures that the adjacent multi-edge toothed cutters on the same roller cooperate closely, and the multi-edge toothed cutter and the roller are assembled by integral key 8.

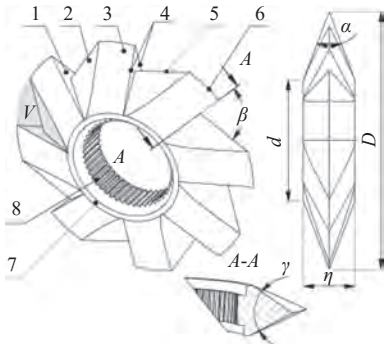

1. Rake face 2. Rear face 3. Flank face 4. Front blade 5. Back blade 6. Top blade 7. Knife hub 8. Integral key

Figure 10 Structure diagram of the multi-edge tooth cutter

The width of the multi-edge toothed cutter η is one of the factors that affect the cutting length of mixed material. When the material is cut by the multi-edge toothed cutter, the theoretical cutting length of the cotton stalk should be the same as the width η. Due to the superior compressibility, flexibility and ductility of the residual film, the theoretical cutting length should be greater than the width η. The difference between the external dimensions of the cotton stalk and the residual film after cutting is conducive to the separation of impurities on the membrane. The mechanism of membrane separation was studied in [10] and [41]. The cotton stalk was crushed to about 50 mm for membrane separation test, and the separation effect was better. As thus, the multi-edge toothed cutter width η was initially determined to be 50 mm. In addition, the outer diameter of the designed multi-edge toothed cutter knife hub was 120 mm, and the side angle α was 40°. In order to ensure a certain strength and service life of the multi-edge gear cutter, the angle γ between the two flanks face was 66°, and the angle β between the rake face and the black blade was 75.5°.

When the rotational speed of the cutting roller and its outer diameter were constant, the straw length decreased gradually with an increase in the number of teeth in the multi-edged toothed cutter[44-46]. Jing[47] suggested that the theoretical width of plastic tearing should be consistent with the tooth width of the counter-roll plastic tearing machine, and the theoretical length of plastic tearing has a certain functional relationship with the number of teeth, the top diameter and bottom diameter of the tearing knife, as follows:

$$l_c = \frac{\pi(D-d)}{z} \tag{16}$$

where, l_c is the theoretical tearing length of plastic, mm; D is the top blade diameter of the multi-edge tooth cutter, mm;. d is the knife hub diameter of the multi-edge tooth cutter, mm; z denotes the tooth number of the multi-edge tooth cutter.

The previous tensile mechanical test of residual film shows that the maximum tensile strain of residual film over a period of half a year was still nearly 4 times the original length of residual film. There were also certain tensile and tear stresses when considering residual film cutting. Therefore, the residual film deformation coefficient λ was introduced to modify Equation (16). The value of λ was 4 and brought into Equation (16) as follows:

$$l_c = \frac{\pi(D-d)}{z} \cdot \lambda \tag{17}$$

Different membrane separation equipment has different requirements for the size of the residual film after cutting. The pre-tests were carried out by the type of pneumatic and interlaced multi-screen as well as disk screen separating device, the results show that the 20-500 mm sized residual film was suitable for membrane separation. The determined value d, value D and the average maximum outer profile size of the residual film were brought to Equation (17), the number of teeth was 6.77, and was rounded to 8.

The top edge of the multi-edge toothed cutter has the cutting effect on the membrane-impurity mixed material. The short arc length l of the top edge was not conducive to cut. Although increasing the arc length l of the top edge would be conducive to improving the cutting effect, the angle of rotation of the uncut residual film with the roller also increased, thereby increasing the winding probability between the residual film and the multi-edge tooth blade. In Figure 11a, when the V-shaped region surrounded by the rake face and the rear faces on both sides remained unchanged, there was a functional relationship among the top edge arc length l and the back blade length l' and the tooth number z:

$$\begin{cases} z = \dfrac{360^\circ}{\tau} \\ l = L - l_1 = \dfrac{\pi r}{180^\circ} \cdot (\tau - \tau_1) \\ l' = r\dfrac{\sin\tau_1}{\sin\beta} \end{cases} \tag{18}$$

where, z is the number of teeth in the multi-edged cutter; T, τ_1 and β are the tooth angle, the central angle of the V-shaped region, and the angle between the rake face and the back blade, (°) respectively (Here τ_1=27.2°); l, L and l_1 are top edge arc length, tooth angle arc length, V region arc length, mm; r is the top edge radius of multi-edge toothed cutter, mm.

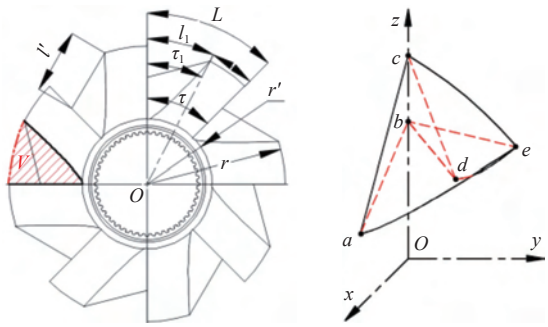

a. Arc length of top edge of multi-edge tooth cutter

b. V-shaped region diagram

Figure 11 Graphics for calculating the arc length and V-shaped region of the top edge of multi-edge tooth cutter

The existence of the V-shaped region on the multi-edge toothed cutter was conducive to the capture, migration and processing of the

cutting device with the multi-edge toothed cutter (Figure 11a). In the cutting process, the material to be processed was continuously extruded to the *V*-shaped region by the interaction of high- and low-speed multi-edge toothed cutter rake faces, and the material was taken to different processing regions. The number and volume of *V*-shaped region had a certain influence on the working efficiency of the cutting device and the material cutting effect, while the number of *V*-shaped region was the same as the tooth number *z*, and the volume of a single *V*-shaped region remained unchanged. With an increase in the tooth number *z*, the number of *V*-shaped regions, rake face, rear face, front blade and back blade of the multi-edge toothed cutter increased, and the arc length of top edge gradually shortened. Although an increase in the number of *V*-shaped regions was conducive to the capture and migration, it reduced the material cutting effect to a certain extent with the gradual shortening of the top edge arc length. When the number of *V*-shaped regions was small, the long arc length of the top edge was beneficial to the cutting of materials, but it would lower the abilities of the multi-edge toothed cutter to grab and migrate materials, thereby resulting in a decline in the working efficiency of the cutting device.

In Figure 11b, the Cartesian coordinate system *O-xyz* was constructed with the center axis of multi-edge toothed cutter rotation, the axis perpendicular to the center axis in the vertical direction and the axis perpendicular to the center axis in the horizontal direction as *x-axis*, *y-axis* and *z-axis*, and the center of multi-edge toothed cutter rotation as the origin *O*. The *V*-shaped region surrounded by *abcde* was symmetrical on both sides according to the plane formed by point *bce*. The volume of *V*-shaped region was calculated by the triple integral method:

$$V' = 2\iiint \mathrm{d}v = 2\int_0^{x'}\int_0^{y'}\int_{z_1}^{z_2} 1\mathrm{d}z\mathrm{d}y\mathrm{d}x \tag{19}$$

where, V' is the volume of the *V*-shaped region, mm^3; x' is the upper limit of the projection integral interval of the *V*-shaped region in the *xOz* plane; y' is the upper limit of the projection integral interval of the *V*-shaped region in the *xOy* plane; z_1 and z_2 are the lower and upper limits of the projection integral interval of the *V*-shaped region in the *yOz* plane, respectively.

The ranges of x', y', z_1 and z_2 in Equation (19) are

$$\begin{cases} x' = \dfrac{\eta}{2} \\ y' = \sqrt{R^2-(x+x_0)^2}-y_0 \\ z_1 = \dfrac{2r'}{\eta\cos\dfrac{\tau_1}{2}} + \dfrac{2x-\eta}{2\tan\dfrac{\gamma}{2}} + \dfrac{r-r'}{2r\sin\tau_1\cos\dfrac{\tau_1}{2}}y \\ \quad -\tan\dfrac{\tau_1}{2}y - \dfrac{\eta}{4r\sin\tau_1\cos\dfrac{\tau_1}{2}\tan\dfrac{\gamma}{2}}y \\ z_2 = \sqrt{\left[\dfrac{2x(r-r')}{\eta}+r\right]^2-y^2} \end{cases} \tag{20}$$

where, η is the width of the multi-edge toothed cutter, mm; *R* is the approximate radius of the curve projected onto the plane *xOy*, mm; x_0 and y_0 are the coordinate values of the approximate radius of the curve projected onto the plane *xOy* relative to the center *O*, mm; r' and *r* are the radius of the knife hub and top edge of the multi-edge gear cutter, mm, respectively; γ is the angle between the two back blades, (°).

In addition, considering machinability, heat treatment technology and processing cost, the multi-edge toothed cutter was made of 40Cr steel. The tensile strength of the material was 810 MPa, the yield strength was 785 MPa, the Poisson's ratio was 0.27, the elastic modulus was 210 GPa, and the density was 7820kg/m^3. In order to improve the surface wear resistance and strength, the cutter blade and surface high frequency quenching, hardness HRC 52-60, the cutting tooth roller shaft was made of 40Cr steel. In order to ensure the strength and toughness of the roller and prevent the integral key wear or fracture caused by excessive disassembly or excessive impact, they were carburized and quenched at a high frequency, and the hardness was HRC 45-50. The rest parts were quenched and tempered, and the hardness was HRC 28-32.

4.3 Design of clearance adjustment mechanism and determination of working parameters

The clearance δ between multi-edge toothed cutters and fixed cutter on high- and low-speed toothed rollers is one of the key factors affecting the cutting length of membrane-impurity mixed material. In Figure 9, the interleaved cutting and extrusion area is formed by the interleaved arrangement of multi-edge toothed cutters on the high- and low-speed toothed rollers. The area has a functional relationship with the center-to-center distance *a* between the high- and low-speed toothed rollers, the radius *r* of the multi-edge toothed cutter and the angle θ of the interleaved area. The θ also has a functional relationship with *a* and *r*, as follows:

$$\begin{cases} S_1 = \dfrac{\theta\pi r^2}{180^\circ} - ar\sin\dfrac{\theta}{2} \\ \theta = 2ar\cos\dfrac{a}{2r} \end{cases} \tag{21}$$

where, S_1 is the staggered cutting extrusion area, mm^2; θ is the angle of the interleaved cutting extrusion area, (°); *r* is the top edge radius of multi-edge toothed cutter, mm; *a* is the center-to-center distance between high- and low-speed toothed rollers, mm.

In Figure 12, there is a functional relationship among the center-to-center distance *a*, the width of the interleaved region a', the top edge radius *r* and the knife hub radius r' of the multi-edge tooth cutter on the high- and low-speed toothed roller, *c* and the clearance δ of the multi-edge tooth cutter, as follows:

$$\begin{cases} c = \dfrac{\delta}{\sin\dfrac{\alpha}{2}} \\ a = r + r' + c \\ a' = r - r' - c \end{cases} \tag{22}$$

where, a' and δ are the gap between the width of the interleaved cutting and extrusion area and the multi-edge toothed cutter, mm; α is the side angle of multi-edge toothed cutter, (°); r' is the knife hub radius, mm; *c* is the spacing between the top edge of the toothed cutter and the outer circle of the cutter knife hub on the two cutting tooth rolls, mm.

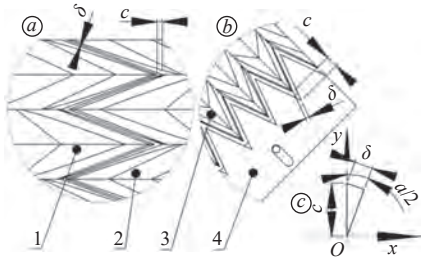

1. Multi-edge toothed cutter on low speed toothed roller 2, 3. Multi-edge toothed cutter on high speed toothed roller 4. Fixed blade

Figure 12 Clearance between the multi-edge tooth cutter and the fixed blade

Since the top edge radius *r*, the knife hub radius r' and the flank angle α of the toothed cutter are fixed values, Equation (21) is

brought to Equation (22). The relationship among the interleaved cutting extrusion area S_I, the interleaved area angle θ and the gap δ of the multi-edge toothed cutter is:

$$\begin{cases} S_I = \dfrac{\theta\pi r^2}{180^\circ} - \left(r + r' + \dfrac{\delta}{\sin\dfrac{\alpha}{2}}\right) r\sin\dfrac{\theta}{2} \\ \theta = 2\arccos\left(\dfrac{r'}{2r} + \dfrac{\delta}{2r\sin\dfrac{\alpha}{2}} + \dfrac{1}{2}\right) \end{cases} \tag{23}$$

It can be seen from Equations (22) and (23) that with an increase in the clearance δ between the toothed cutters, the center-to-center distance a between the two cutting toothed rollers gradually increases. The width a', the area S_I, and the angle θ of the interleaved extrusion region gradually decrease, resulting in the weakening of the cutting and extrusion effect between the multi-edge toothed cutters and the reduction of the cutting power consumption. The residual film and cotton stalk were not completely cut, and the cotton stalk with diameter less than the clearance δ between the multi-edge toothed cutters was directly discharged, and the cutting effect of the membrane-impurity mixed material was poor.

When the gap δ between the multi-edge toothed cutters decreases, the center-to-center distance a between the high- and low-speed toothed cutters decreases gradually, the width a' and I area S_I of the interleaved extrusion area increase gradually, the cutting and extrusion effect between the multi-edge toothed cutters increases, which improves the cutting effect of the membrane-impurity mixed material. In addition, when the clearance δ was small, although it was conducive to the cutting of membrane-impurity mixed material, the cutting power consumption was also improved. In addition, too small clearance δ would increase the possibility of collision, damage the device, and even cause casualties[48,49].

Further, the gap between the multi-edge toothed cutter and the fixed blade and the gap δ between the multi-edge toothed cutters had the same cutting effect on the film mixture, and the film removal effect was weakened when the gap between the multi-edge toothed cutter and the fixed cutter was large, which was easy to cause residual film and roller winding. According to the sorting test of mixed material, the mass of cotton stalks with lengths of [0,50) mm, [50,100) mm and [100,~) mm accounted for (26.88±5.81)%, (40.72±7.51)% and (32.74±7.12)%, respectively. Therefore, the clearance δ between multi-edge toothed cutters and between multi-edge toothed cutters and fixed blade was preliminarily determined to be 3mm.

As shown in Figure 13a, the clearance adjustment mechanism between multi-edge toothed cutters is mainly composed of slide bearing, bolts and nuts. By adjusting the position of the slide bearing, the center-to-center distance a of the high- and low-speed toothed rollers can be adjusted (Figure 9), so as to achieve the purpose of adjusting the clearance between the multi-edge toothed cutters on the two toothed rollers. As shown in Figure 13b, the fixed cutter seat uses the fixed cutter bolt to connect with the inner wall of the cutting cavity of the device. By adjusting the relative position between the fixed blade seat and the fixed blade, the gap adjustment between the fixed blade and the multi-edge toothed cutter can be realized.

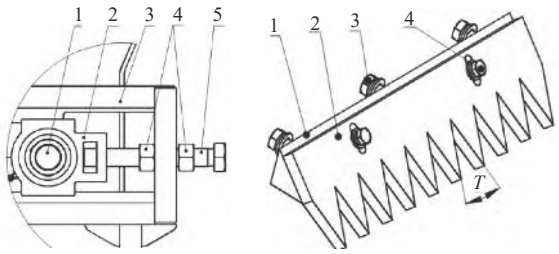

1. Low-speed toothed roller 2. Bearing 3. Frame 4. Nut 5. Bolt
a. Gap adjustment mechanism between multi-edge toothed cutters

1. Fixed blade seat 2. Fixed blade 3. Fixed lade bolt 4. Clearance adjustment bolt
b. Gap adjustment mechanism between multi-edge toothed cutter and fixed blade

Figure 13 Clearance adjusting mechanism

4.4 Modal numerical analysis of cutting toothed roller

When the membrane-impurity mixed material was cut, the high-speed toothed roller was prone to vibrate, and resonance would cause fatigue damage to structural components, affect normal use, and easily cause safety accidents. Therefore, the finite element software ANSYS was employed to analyze the modes of high- and low-speed toothed rollers, obtain the natural frequency and maximum displacement deformation, and test the safety.

The model of high- and low-speed toothed rollers built by SolidWorks was imported into the modal module of finite element software ANSYS. The model material properties were set according to the properties of 40Cr steel. The SOLID92 grid type was selected to divide the grids of two toothed rollers, and the fixed hinges were added at both ends of the roller. The simulation results are shown in Table 1 and Figure 14.

Table 1 Eight-order modal analysis results of high- and low-speed toothed roller

Order	High-speed toothed roller		Low-speed toothed roller	
	Oscillation frequency/Hz	Maximum deflection/mm	Oscillation frequency/Hz	Maximum deflection/mm
1	250.33	4.22	237.82	4.46
2	250.99	4.22	238.78	4.47
3	358.74	5.96	337.59	6.36
4	852.81	6.13	796.46	6.22
5	854.54	6.12	799.85	6.21
6	1385.8	4.18	1219.8	4.09
7	1673.4	8.11	1367.1	8.57
8	1778.8	6.72	1713.3	6.85

In Table 1, the natural frequencies of the first eight modes of the high-speed toothed roller fell in the range of 250.33-1778.8 Hz, and the maximum displacement deformation was in the range of 4.18-8.11 mm. The natural frequency of the eighth mode was the highest, and the displacement deformation of the seventh mode was the largest. It can be seen from Figure 14a that except for the deformation on the left side of the high-speed toothed roller in the eighth order vibration mode, the deformation in the other order vibration modes was at the first tooth cutter on the left side. In the second, third, sixth and seventh vibration modes, the overall circumferential displacement deformation of the high-speed toothed roller was larger. Under the remaining order vibration mode, the axial displacement deformation was larger.

As shown in Table 1, the first eight natural frequencies of the low-speed toothed roller were in the range of 237.82-1713.3 Hz, and the maximum displacement deformation was in the range of 4.09-8.57 mm. The natural frequency of the eighth mode was the highest, and the displacement deformation of the seventh mode was the largest. From Figure 14b, the displacement and deformation position of the low-speed toothed roller was the same as the high. In addition to the deformation on the left side of the low-speed toothed

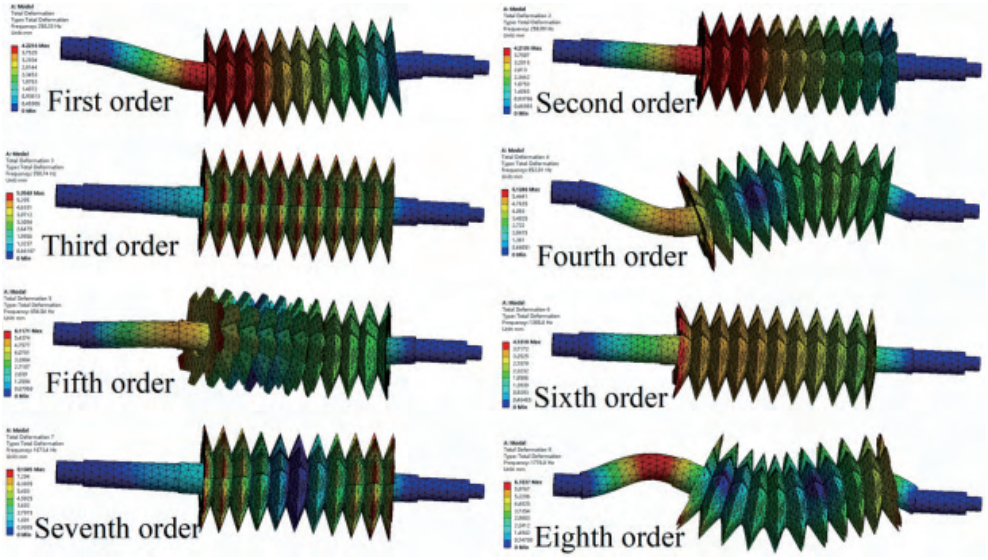

a. Modal analysis results of the first eight modes of high-speed toothed roller

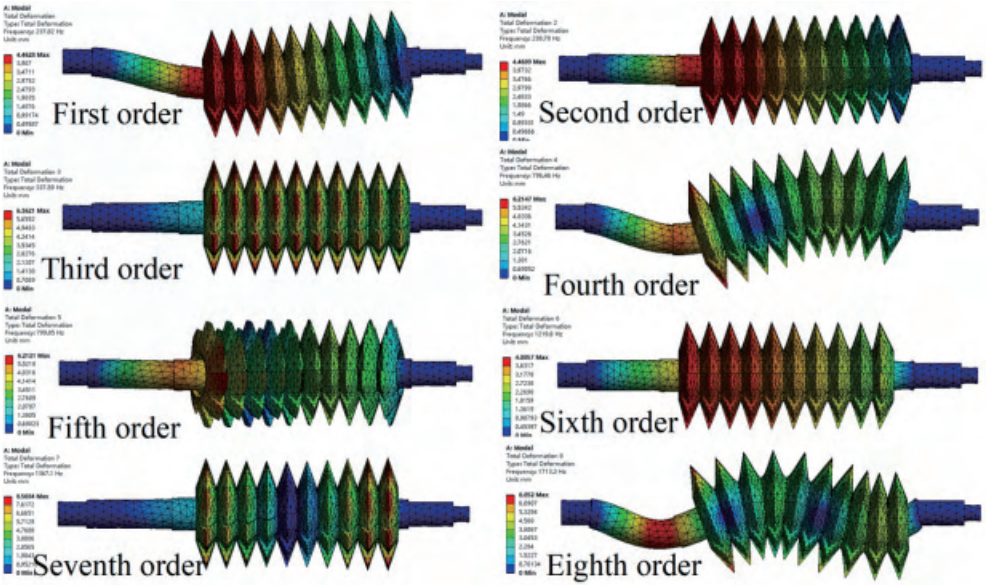

b. Modal analysis results of the first eight modes of low-speed toothed roller

Figure 14 Modal analysis results of the first eight order vibration modes of high- and low-speed toothed roller

roller under the eighth order vibration mode, the deformation in the other order vibration mode was at the first toothed cutter on the left side. In the first, fourth and eighth order vibration modes, the overall circumferential displacement deformation of the low-speed toothed roller was large, while the axial displacement deformation was large in the number of vibration modes.

The rotational speed of the high- and low-speed toothed rollers determined in Section 3.1 was to be solved by Equation $f=n/60$[50]. The excitation frequencies of the two toothed rollers were 13.33 Hz and 8.33 Hz, respectively, which were far smaller than the natural frequencies of the first eight modes, indicating that no resonance occurred between the two toothed rollers at work.

5 Performance test

5.1 Test materials and instruments

The test took place in mid-October 2020 in the Northwest Key Laboratory of Agricultural Equipment, Ministry of Agriculture and Rural Affairs, Shihezi University. The test materials were collected in late September 2020 from the surrounding farms in Shihezi City, Xinjiang (Figure 15a). Before the test, the basic physical parameters of the membrane-impurity mixed material were determined. The test results show that the ratios of the mass of granular materials dominated by soil, the mass of unwashed residual membrane, and the mass of cotton stalk to the total mass of membrane-impurity mixed material were 48.99%, 15.12% and 35.89%, respectively. The moisture contents of cotton stalks and granular materials in the sample were (19.02±5.52)% and (8.82±3.07)%, respectively. When the membrane-impurity mixed material was cut, the particle size of

a. Membrane-impurity mixed material b. Cutting device

Figure 15 Membrane-impurity mixed material and its cutting device

the granular material mainly composed of soil was eliminated because of its small size and it was easy to cause dust pollution.

The test instruments were mainly Sartorius MA100 electronic moisture meter (mass accuracy: 0.001 g, moisture content accuracy: 0.01%, Germany Sedolis), JMB5003 electronic balance (measurement range: 0-00 g, measurement accuracy: 0.001 g, Zhejiang Yaojiming weighing calibration equipment Co., Ltd.), TCS-60 electronic platform scale (measurement range: 0-100 kg, measurement accuracy: 2 g, Guangdong Zhongshan Hengyu Electronic Instrument Co., Ltd.), HCNJ-101 dynamic torque sensor (range: 0-500 N·m, accuracy: ±0.5%, Beijing Haibohua Science and Technology Co., Ltd.), DL91150 digital vernier caliper. The test device was a self-built multi-edge toothed cutting device for membrane-impurity mixed material, as shown in Figure 15b.

5.2 Test methods and assessment indicators

The number z of multi-edge toothed cutter teeth of the cutting device was set to be 8; the gap between the multi-edge toothed cutter and the fixed blade δ was 3 mm; the speed of the high-speed toothed roller n_1 was 800 r/min, and the speed difference Δn between the high- and low-speed toothed rollers was –300 r/min. In the physical test, the membrane-impurity mixed material was first evenly laid on the feed conveyor belt, and the device was /started. After it ran stably, the feed conveyor belt was started again. Due to the large volume and fluffy of the membrane-impurity mixed material, when the material feeding amount was too large or the feeding speed was too fast, it was easy to cause the crushing device to block, forming an overload and causing an instantaneous shutdown. Therefore, according to the pre-test, the material processing capacity of each group was set to be (2.0±0.1) kg, the feeding speed was 0.01 m/s, and the material was fed to the complete discharge during the effective working period of the material processing.

After the test, according to GB/T26551-2011 in the cross-sampling method, each group had a sample mass of (400±10) g. After sampling, the residual film and cotton stalk in the crushed film mixture were manually sorted, and the total mass of the residual film and cotton stalks was recorded. It was unable to collect small-sized materials that were counted in the minimum distribution range.

(1) Distribution characteristics of the maximum outline size of residual film

The maximum outline size of residual film was classified according to the four distribution ranges of [0,20) mm, [20,100) mm, [100,500) mm and [500,~) mm. After material classification, the JMB5003 electronic balance was used to weigh the material in each range. The ratio of material quality to material sampling quality in each distribution range was

$$\begin{cases} x_1 = \dfrac{m_1}{m} \times 100\%; \quad x_2 = \dfrac{m_2}{m} \times 100\% \\ x_3 = \dfrac{m_3}{m} \times 100\%; \quad x_4 = \dfrac{m_4}{m} \times 100\% \end{cases} \tag{24}$$

where, m, m_1, m_2, m_3 and m_4 are the sampling quality of residual film respectively, and the quality of residual film was in the range of [0,20) mm, [20,100) mm, [100,500) mm and [500,~) mm, g; x_1, x_2, x_3, x_4 are the ratio of m_1, m_2, m_3, m_4 to m, %.

(2) Distribution characteristics of cotton stalk length

Cotton stalk length was classified according to the three distribution ranges of [0,50) mm, [50,100) mm and [100,~) mm. The ratio of cotton stalk quality to sampling quality in different length distribution ranges is:

$$y_1 = \frac{M_1}{M} \times 100\%; \quad y_2 = \frac{M_2}{M} \times 100\%; \quad y_3 = \frac{k_3}{M} \times 100\% \tag{25}$$

where, M, M_1, M_2 and M_3 are the quality of cotton stalk samples, respectively, in the range of [0,50) mm, [50,100) mm and [100,~) mm, g; y_1, y_2 and y_3 are the ratios of M_1, M_2 and M_3 to M, respectively, %.

(3) Cutting power consumption

When considering cutting power consumption, the dynamic torque sensor installed on the device was utlized to measure power consumption. After the test, the collected instantaneous power was exported. Referencing the literature [46], the data processing software Origin was used to calculate the cutting power consumption for the instantaneous power integral in the effective working period.

$$w = \frac{\sum_{i=1}^{n} \int [P_g(t) + P_d(t)] \mathrm{d}t_s}{n} \tag{26}$$

where, w is the cutting power consumption per unit mass, kJ; $P_g(t)$ and $P_d(t)$ are the instantaneous power of high- and low-speed toothed rollers, respectively, kW; t_s is the effective working time, s; n is the mass of the membrane-impurity mixed material, kg.

5.3 Analysis of test results

The effect of residual film and cotton stalks in the membrane-impurity mixed material after cutting is shown in Figure 16, and the test data are listed in Table 2.

a. Cutting effect of residual film b. Cutting effect of cotton stalk

Figure 16 Cutting effect of residual film and cotton stalk

Table 2 Statistical table of test assessment indicators

Index	1	2	3	4	5	Mean value
x_1/%	2.6	1.75	2.19	2.34	2.22	2.22±0.31
x_2/%	18.9	20.02	17.39	19.58	15.04	19.19±2.02
x_3/%	55.55	59.38	62.1	55.76	61.91	58.94±3.19
x_4/%	22.95	18.85	18.32	22.32	20.83	20.65±2.05
y_1/%	31.99	32.03	34.87	30.88	33.1	32.57±1.5
y_2/%	28.52	27.45	26.21	27.1	29.56	27.77±1.3
y_3/%	39.49	40.52	38.92	42.02	37.34	39.66±1.75
W/kJ	97.15	105.61	75.89	67.54	80.85	85.41±15.63

Table 2 presents that the average ratios of residual film mass to residual film sampling mass x_1, x_2, x_3 and x_4 are (2.22±0.31)%, (19.19±2.02)%, (58.94±3.19)% and (20.65±2.05)%, respectively, when the maximum outer dimensions are in the ranges of [0,20) mm, [20,100) mm, [100,500) mm and [500,~) mm. It can be seen that the mass of residual film with the maximum profile size in the range of (20,500] mm accounts for about 78.13% of the sample mass of residual film. In this distribution area, the residual film can be separated by air separation and suspension methods. When the suspension method was used for separation, the smaller residual film was easy to adhere to the inner wall of the washing device, and the small residual film was easy to cause secondary pollution with the discharge of water. The residual film mass with the maximum

outer profile size in the range of [0,20) mm should be reduced as far as possible. When the size of the cut cotton stalk was large, the residual film within the range of [500,~) mm would still be intertwined with the longer cotton stalk (<100 mm), or the impurities with smaller particle size would be wrapped, which affected the separation effect of membrane-impurity mixed material, and it was necessary to conduct secondary cutting.

The average values of the ratios y_1, y_2 and y_3 of cotton stalk mass to cotton stalk sampling mass in the ranges of [0,50) mm, [50,100) mm and [100,~) mm were (32.57±1.5)%, (27.77±1.3)% and (39.66±1.75)%, respectively. Clearly, the ratio of cotton stalk quality to cotton stalk sampling quality was close in the above three intervals. As cotton stalk length fell in the range of [100,~) mm and the maximum outer size of the larger residual film would still be entangled, it was not conducive to separating membrane-impurity mixed material and secondary cutting should be conducted. When the cotton stalk length was in the range of [0,50) mm and [50,100) mm, the separation can be realized by suspension method or air separation method.

Besides, the cutting power consumption range was (67.54-105.61) kJ, and the average cutting power consumption was (85.41±15.63) kJ. Due to the complex structure characteristics, disordered distribution of membrane-impurity mixed material and different mixing ratios, the cutting power consumption between different groups was different, which was the main reason for the high standard deviation of cutting power consumption. On this basis, the cutting mechanism of membrane-impurity mixed material will be further studied to find out the influence of cutting characteristics of membrane-impurity mixed material.

6 Conclusions

Combined with the characteristic of membrane-impurity mixed material, the compressive and cutting force characteristics of residual film material layer and cotton stalk were analyzed, the cutting conditions of membrane-impurity mixed material were obtained, and the method of cutting was determined. A multi-edge toothed cutter was developed, and the physical model of the toothed cutting device was established. The key parameters of the cutting device were determined, and the physical test was carried out to verify the feasibility of the cutting method, the conclusions of this study are as follows:

1) Taking cotton stalks and residual film material layers as the research objects, combined with the properties of the two materials, the cutting conditions of the two materials were analyzed. The results show that: the stress and energy required for cutting cotton stem are mainly concentrated in the cutting and deformation stage. The compression time of the residual film layer is long and the compression deformation is large, and the characteristics of cotton stalk and the residual film material, and the frictional characteristic, as well as the cutting tool structure will affect the cutting. Analysis of residual film layer and cutting condition of cotton stalk, which provided conditions for the design and parameter determination of the multi-edge toothed cutting device for membrane-impurity mixed material.

2) Based on the analysis of the cutting conditions of the membrane-impurity mixed material, the structural and working characteristics of the multi-edge toothed cutting device for membrane-impurity mixed material were described, and the key components of the device were designed. At the same time, it was preliminarily determined that the number of multi-edge toothed cutter teeth z was 8, the gap between the multi-edge toothed cutter and the fixed blade δ was 3 mm, the speed of the high-speed toothed roller n_1 was 800 r/min, and the speed difference between high- and low-speed toothed rollers Δn was –300r/min.

3) The cutting test results show that the residual film mass with the maximum outer profile size in the range of [20,500] mm accounted for about 78.13% of the residual film sampling mass, and the cotton stalk mass with the length of [0,100) mm accounted for about 60.34% of the cotton stalk sampling mass. The cutting power consumption of the test device was (85.41±15.63) kJ, indicating that the performance of the cutting device was feasible. The cutting mechanism was deeply studied to reveal the influence of cutting characteristics of membrane-impurity mixed material.

Acknowledgements

This study was financially supported by the Fund for Less Developed Regions of the National Natural Science Foundation of China (Grant No. 52065058), Graduate Education Innovation Project of Xinjiang Uygur Autonomous Region (Grant No. Xj2022G085), the Key Industry Innovation Development Support Plan of South Xinjiang (Grant No. 2020DB008), the Open Fund of Jiangsu Province and Education Ministry Co-sponsored Synergistic Innovation Center of Modern Agricultural Equipment (Grant No. XTCX2006), Scientific and technological innovation team of Xinjiang Production and Construction Corps (Grant No. 2020CB013).

[References]

[1] Luo H, Zhang Y, Zhang W. Effects of water stress and rewatering on photosynthesis, root activity, and yield of cotton with drip irrigation under mulch. Photosynthetica:International Journal for Photosynthesis Research, 2016; 54(1): 65–73.

[2] Wang Z, Wu Q, Fan B, Fan B, Zhang J, Li W, et al. Testing biodegradable films as alternatives to plastic films in enhancing cotton (*Gossypium hirsutum* L.) yield under mulched drip irrigation. Soil and Tillage Research, 2019; 192: 196–205.

[3] He H, Wang Z, Guo L, Zheng X, Zhang J, Li W, Fan B. Distribution characteristics of residual film over a cotton field under long-term film mulching and drip irrigation in an oasis agroecosystem. Soil & Tillage Research, 2017; 180: 194–203.

[4] Ileana B, Viviana L R, Carmela S, Evelia S, Giuliano V. Agricultural plastic waste mapping using GIS. A case study in Italy. Resources, Conservation and Recycling, 2018; 137: 229–242.

[5] Liang R, Chen X, Zhang B, Meng H, Jiang P, Peng X, et al. Problems and countermeasures of recycling methods and resource reuse of residual film in cotton fields of Xinjiang. Transactions of the CSAE, 2019; 35(16): 1–13. (in Chinese)

[6] Sheriff K, Subramanian N, Rahman S, Jayaram J. Integrated optimization model and methodology for plastics recycling: Indian empirical evidence. Journal of Cleaner Production, 2016; 153(1): 707–717.

[7] Rahim R, Raman A. Carbon dioxide emission reduction through cleaner production strategies in a recycled plastic resins producing plant. Journal of Cleaner Production, 2017; 141(10): 1067–1073.

[8] Zhang J, Wang X, Zhang L, Yu C, Jiang Y, Zhang H, et al. Effects of mechanical tensile properties of plastic film on plastic recycling method. Transactions of the CSAE, 2015; 31(20): 41–47. (in Chinese)

[9] Jiang D, Chen X, Yan L, Mo Y, Yang S. Design and experiment on spiral impurity cleaning device for profile modeling residual plastic film collector. Transactions of the CSAM, 2019; 50(4): 137–145. (in Chinese)

[10] Shi X, Niu C, Wang X, Zhang H, Yang H. Design of roller sieve waste plastic film and trash winnowing machine. Transactions of the CSAE, 2017; 33(18): 19–26. (in Chinese)

[11] Li J, Luo X, Hu B, Wang M, Yao Q. Research and experiment of the water-separating device for residual film mixture. Journal of Agricultural Mechanization Research, 2019; 41(5): 152–156. (in Chinese)

[12] Peng Q, Li C, Kang J, Shi G, Zhang H. Improved design and test on pneumatic cylinder sieve film hybrid separator. Transactions of the CSAM, 2020; 51(8): 126–135. (in Chinese)

[13] Pan F, Hu B, Luo X, Guo M, He H. Design and testing of a shearing and breaking device for mulch film and cotton stalk mixtures. Transactions of the ASABE, 2021; 64(2): 545–555.
[14] Liang R Q, Zhang B C, Zhou P F, Li Y P, Meng H W, Kan Z. Power consumption analysis of the multi-edge toothed device for shredding the residual film and impurity mixture. Computers and Electronics in Agriculture, 2022; 196: 106898.
[15] Liang R Q, Zhang B C, Zhou P F, Li Y P, Meng H W, Kan Z. Cotton length distribution characteristics in the shredded mixture of mechanically recovered residual films and impurities. Industrial Crops and Products, 2022; 182: 114917.
[16] Ádám R, Barnabás C. Comminution of single real waste particles in a swing-hammer shredder and axial gap rotary shear. Powder Technology, 2021; 390: 182–189.
[17] Geng D, Zhang D, Wang X, Yang Z. New agricultural machinery. Beijing:National Defense Industry Press, 2011; 231p. (in Chinese)
[18] Chu X. Design and experimental research of cutting key device for collection potato stalk. Beijing: China Agricultural University, 2017. (in Chinese)
[19] Johnson K. Contact mechanics. Beijing: Higher Education Press, 1992.
[20] Kanafojski C. Agricultural machines, theory and construction. Beijng: China Agricultural Machinery Publishing House. 1983: 24–30.
[21] Wu J, Wang J, Huang Y. Dynamic analysis on straight knife cutting cotton stalks. Journal of Shihezi University (Natural Science), 2005; 6: 752–754. (in Chinese)
[22] Zou X, Niu W, Liu J, Li Y, Liang B, Guo L, Guan Y. Effects of residual mulch film on the growth and fruit quality of tomato (*lycopersicon esculentum* mill.). Water Air & Soil Pollution, 2017; 228(2): 1–18.
[23] Qi A, Du C. Mechanics (Second Edition). Beijing:Higher Education Press, 1997; 266–269. (in Chinese)
[24] Sonde V, Belkhode P, Sakhale C. Physical and mechanical characteristic for cotton and pigeon pie as agriculture residues. International Journal of Application or Innovation in Engineering & Management, 2015; 4(7): 156–169.
[25] Wang M, Song W, Xiao H, Ren C, Li S. Design and experiment of 9MF720 cotton stalk crusher. Journal of Agricultural Mechanization Research, 2012; 34(11): 94–96, 101. (in Chinese)
[26] Yu C, Zhang L, Zhao Z, Li Y, Zhang H, Jiang Y, Zhang J. Structural design and optimization of cotton straw rubbing filament crusher. Journal Chinese Agricultural Mechanization, 2016; 37(7): 93–96. (in Chinese)
[27] Liao P, Liu K, Chen M, Wang Z, Zhang A. Design and experiment of a roller type cotton stalk cutting mechanism. Journal of China Agricultural University, 2018; 23(9): 131–138. (in Chinese)
[28] Sheng K, Ahmed E, Hassan G. Experimental studies on chopping cotton stalk and briquetting process. Transactions of the CSAE, 1999; 15(4): 221–225. (in Chinese)
[29] Dong S, Wang F, Qiu Z, Sun Y. Design and experiment of Self-propelled cotton-stalk combine harvester. Transactions of the CSAM, 2010; 41(S1): 99–102. (in Chinese)
[30] Luo S, Xiao B, Hu Z, Liu S, Guo X. An experimental study on a novel shredder for municipal solid waste (MSW). International Journal of Hydrogen Energy, 2009; 34(3): 1270–1274.
[31] Sakai S, Sawell S, Chandler A, Eighmy T, Hjelmar O. World trends in municipal solid waste management. Waste Management, 1996; 16(5-6): 341–350.
[32] Vincent G, Bruijn T, Wijskamp S, Rasheed M, Akkerman R. Shredding and sieving thermoplastic composite scrap: Method development and analyses of the fibre length distributions. Composites Part B Engineering, 2019; 176: 107197.
[33] Maisel F, Chancerel P, Dimitrova G, Emmerich J, Nissen N, Schneider R. Preparing WEEE plastics for recycling - how optimal particle sizes in pre-processing can improve the separation efficiency of high quality plastics. Resources, Conservation and Recycling, 2020; 154: 104619.
[34] Xue Z, Fu J, Chen Z, Wang F, Han S, Ren L. Optimization experiment on parameters of chopping device of forage maize harvester. Journal of Jilin University:Engineering and Technology Edition, 2020; 50(2): 739–748. (in Chinese)
[35] Chinese Academy of Agricultural Mechanization Sciences. Agricultural machinery design manual (Second volume). Beijing:China Agricultural Science and Technology Press, 2007; 1182. (in Chinese)
[36] Tosun A, Konak G. Development of a model estimating energy consumption values of primary and secondary crushers. Arabian Journal of Geosciences, 2015; 8(2): 1133–1144.
[37] Sun N, Wang X, Li H, He J, Wang Q, Wang J, Liu Z, Wang Y. Design and experiment of differential sawing rice straw chopper for turning to field. Transactions of the CSAE, 2019; 35(22): 267–276. (in Chinese)
[38] Wan X, Shu C, Xu Y, Yuan J, Li H, Liao Q. Design and experiment on cylinder sieve with different rotational speed in cleaning system for rape combine harvesters. Transactions of the CSAE, 2018; 34(14): 27–35. (in Chinese)
[39] Chen H, Teng Y, Wang Y, Shi N, Wang X. Design and experiment on single-plant soybean threshing device with differential speed flexible belts. Transactions of the CSAM, 2018; 49(9): 96–104. (in Chinese)
[40] Ruan J, Xiang G, Cheng X. Experiments and optimization of performance parameters on rubber roll husker. Transactions of the CSAE, 2011; 27(5): 353–357. (in Chinese)
[41] Liu P, He J, Li Y, Li H, Wang Q, Lu C, et al. Design and experiment of double rollers maize stalk chopping device with different rotation speeds. Transactions of the CSAE, 2020; 36(14): 69–79. (in Chinese)
[42] Mou X, Jiang H, Sun Y, Xu H, Yao Y, Geng D. Simulation optimization and experiment of disc-type grain crushing device of silage corn harvester. Transactions of the CSAM, 2020; 51(S1): 218–226. (in Chinese)
[43] Kang J, Zhang H, Zhang G, Du H, Peng Q, Song Y. Aerodynamic characteristics of residual film materials and test of membrane separation device. Journal of Chinese Agricultural Mechanization, 2020; 41(1): 167–172. (in Chinese)
[44] Yu Y, Zhang J, Geng A, Zhang Z, Yang Q, Zhang J. Design and test of roller strip chopping device. Journal of Agricultural Mechanization Research, 2019; 41(3): 93–98. (in Chinese)
[45] Zhang D, Sun Y, Zhao H, Wang X. Design of a vertical-roll type of corn picker and stalk chopper. Transactions of the CSAM, 2005; 36(7): 50–52, 76. (in Chinese)
[46] Jiang Y, Liao Y, Liao Q. Design and experiment on cylinder-type chopping device of harvester for fodder rapeseed in winter and spring. Transactions of the CSAM, 2019; 50(2): 102–111. (in Chinese)
[47] Jing S W. Design and performance test of key components of field membrane hybrid separation system. Guiyang:Guizhou University, 2018; 34–35. (in Chinese)
[48] Qiu J, Wu M, Guang C, Fang Y, Li X. Design and experiment of chopping device with dynamic fixed knife coaxial for rice straw. Transactions of the CSAE, 2015; 31(10): 11–19. (in Chinese)
[49] Li W, Dong X, Wang D, Han Z, Cao H, Wu H. Performance experiment of helix teeth-roller straw adjusting material device. Transactions of the CSAM, 2011; 42(12): 143–147. (in Chinese)
[50] Fu M, Li R, Ma L. Development and test of straw grinder with axial vibration screen type. Transactions of the CSAE, 2012; 28(22): 16–22. (in Chinese)